PNAS RESEARCH ARTICLE | PLANT BIOLOGY OPEN ACCESS

A synthetic ERFVII-dependent circuit in yeast sheds light on the regulation of early hypoxic responses of plants

Mikel Lavilla-Puerta[a,b], Yuming He[b], Luca Piccinini[a], Lorenzo Di Paco[a], Antonis Papachristodoulou[c], Francesco Licausi[b,1], and Beatrice Giuntoli[d,1]

Edited by Julia Bailey-Serres, University of California, Riverside, CA; received September 1, 2025; accepted January 29, 2026

Plants face hypoxic conditions either chronically, as particular tissues are characterized by fluctuating or stable low oxygen levels, or acutely, when flooded. In vascular plants, transcriptional adaptive responses to hypoxia are rapidly mounted by Ethylene Response Factors VII (ERFVIIs), regulated by Plant Cysteine Oxidases (PCOs) through the cysteine branch of the N-degron pathway (Cys-NDP) for oxygen sensing. However, this relatively simple regulatory circuit, consisting of both constitutively expressed as well as hypoxia-inducible ERFVIIs and PCOs, interacts with diverse signaling cues and pathways invoked by hypoxia. To understand the share of the PCO-mediated oxygen sensing mechanism in the production of hypoxia responses, we insulated the PCO/ERFVII circuit from *Arabidopsis thaliana* and adapted it to *Saccharomyces cerevisiae*. Using a reporter gene to monitor the output of the circuit allowed us to compare the speed and amplitude of response to hypoxia in the engineered yeast and the source organism. Hypoxia triggered ERFVII stabilization both in Arabidopsis and yeast, leading to a similarly fast transcriptional response that was however larger in plants. A simple hypoxia-inducible feedback loop improved the amplitude of response in yeast, demonstrating the importance of this regulation in the endogenous PCO/ERFVII circuit. Finally, computational modeling of the yeast circuit enabled us to identify promoter competition and presence of hypoxia-inducible PCOs as key parameters that shape early hypoxia responses in plant cells.

Arabidopsis thaliana | hypoxia | *Saccharomyces cerevisiae* | synthetic biology | N-degron pathway

Significance

We report the design, testing and optimization of a synthetic molecular switch that activates gene expression in response to hypoxia in the yeast *Saccharomyces cerevisiae*. This is based on enzymes that consume molecular oxygen to regulate the stability of transcription factors (TFs) in plant cells. By generating such a hybrid molecular device, we were able to demonstrate the efficacy of this hypoxia response strategy independently of the many ancillary components that affect gene regulation in plant cells. In this way, we were able to assess its activation dynamics, characterized by similarly fast induction of gene expression in both yeast and plants. Our approach also revealed the requirement of interlocked feedback loops to achieve the magnitude of gene induction measured in plants.

The enrichment of Earth's atmosphere with molecular oxygen dramatically changed the planet's biogeochemistry and likely impacted on the diversification of life forms (1). Aerobic organisms use this compound for several essential metabolic reactions, including cellular respiration, although they are regularly exposed to fluctuations in oxygen levels (2). Therefore, all aerobes have developed mechanisms to monitor the availability of oxygen and initiate transcriptional responses when its levels fall below their metabolic requirements (hypoxia). Fungi indirectly rely on the abundance of metabolites whose synthesis requires O_2, like sterols or heme (3, 4). Plants and animals converged instead on transcription factors (TFs) whose abundance is posttranslationally controlled in an O_2-dependent fashion (2).

In flowering plants, the response to hypoxia is largely mediated by TFs belonging to the group VII of Ethylene Response Factors (ERFVIIs) (5, 6). ERFVII families from Angiosperms present a variable number of members that, while all participating to low oxygen responses, differ in terms of hypoxia-inducibility and appear to be partially not redundant in activity (5, 7, 8). Most ERFVII proteins are subjected to a common mechanism for O_2-dependent regulation, controlled by the proteolytic N-degron pathway (9, 10). Their N-terminal cysteine, exposed upon cotranslational methionine cleavage by Met aminopeptidases (MetAP) (11) is aerobically oxidized into its sulfinyl ($CysO_2$) or sulfonyl form (CyO_3) by Plant Cysteine Oxidases (PCOs) (12, 13). Oxidation in turn stimulates N-terminal arginine conjugation by arginyltransferase enzymes (ATEs) and subsequent polyubiquitination of proximal Lys by ubiquitin ligases (PRT6 and BIG) (14), before the ERFVIIs are degraded by the proteasome. This series of reactions constitutes the so-called PCO- or Cys-branch of the N-degron pathway, which also enables oxygen perception in metazoan animals (15).

Beyond ERFVII conditional O_2-dependent degradation, additional mechanisms associated with hypoxia impact on the stability or activity of these TFs (*SI Appendix*, Fig. S1). First, mitochondrial retrograde signaling promotes ERFVII stabilization and the consequent activation of hypoxia responsive genes (16). Second, fatty acid desaturation favors ERFVII detachment from the plasma membrane and their relocation to the nucleus (17, 18), in cells where they are protected from degradation. Reduced ATP levels under hypoxia

Author affiliations: [a]Institute of Plant Sciences, Scuola Superiore Sant'Anna, Pisa 56127, Italy; [b]Department of Biology, University of Oxford, Oxford OX1 3RB, United Kingdom; [c]Department of Engineering Science, University of Oxford, Oxford OX1 3PJ, United Kingdom; and [d]Department of Biology, University of Pisa, Pisa 56127, Italy

Author contributions: M.L.-P., A.P., F.L., and B.G. designed research; M.L.-P., Y.H., L.P., and L.D.P. performed research; M.L.-P., Y.H., L.D.P., and B.G. analyzed data; and M.L.-P., Y.H., A.P., F.L., and B.G. wrote the paper.

The authors declare no competing interest.

This article is a PNAS Direct Submission.

[1]To whom correspondence may be addressed. Email: francesco.licausi@biology.ox.ac.uk or beatrice.giuntoli@unipi.it.

This article contains supporting information online at https://www.pnas.org/lookup/suppl/doi:10.1073/pnas.2524358123/-/DCSupplemental.

Published March 10, 2026.

have been connected to a shift of fatty acid composition toward oleoyl-CoA in Arabidopsis seedlings (19). Finally, it has been found that ERFVII phosphorylation in response to early Ca^{2+} signaling or TOR-mediated energy signaling stimulate stabilization and transactivation capacity (20, 21).

Recently, a subset of ER-tethered NAC TFs has been connected to low-oxygen stress responses in *Arabidopsis thaliana* (22, 23). Among them, ANAC013 relocates to the nucleus in the initial phases of hypoxia and associates to core anaerobic gene promoters (24) by contacting their cognate DNA element. Although their role is yet to be fully understood, ANACs have been proposed to cooperate with the ERFVII in the regulation of hypoxia-inducible genes, in response to mitochondrial dysfunction signals (25).

The network of signaling mechanisms invoked by hypoxia, together with the genetic redundancy of their components, raises the question as to whether the cellular response to hypoxia is directly initiated by a decrease in oxygen levels, or, alternatively, it requires the cooperation between the O_2-sensing pathway and indirect signaling of hypoxia. It also remains to be defined how much the transcriptional adjustments to hypoxia can be explained in terms of PCO-mediated ERFVII activity and how much additional pathways contribute to this process. To address these fundamental questions, we resorted to the principles of synthetic biology (26). We reconstructed the ERFVII-dependent transcriptional regulation de novo in baker's yeast (*Saccharomyces cerevisiae*), a chassis that promises to minimize the crosstalk between the synthetic circuit and endogenous regulation. Indeed, yeast oxygen perception operates via heme- and ergosterol-dependent pathways (3, 4) and no PCO or ERFVII homologues exist (27). We have previously demonstrated that a plant-inspired Cys N-degron pathway can be established in yeast (27); here, we introduced the PCO/ERFVII signaling module to regulate gene expression.

Abstraction of plant modules, in a cellular context unhindered by cross-regulating mechanisms, provided us with the opportunity to measure the contribution of the Cys N-degron pathway to the initiation and maintenance of the hypoxic response. Moreover, we could use the quantitative output data from the synthetic yeast to build a model summarizing the properties of a minimal PCO/ERFVII oxygen-dependent circuit. This approach complements the information on the features of plant oxygen sensing obtained so far, through the in vitro characterization of PCO enzymes (12) and *in planta* assessment of gene dynamics (5).

Results

Plant Cells Rapidly Mount Fast Transcriptional Responses to Acute Hypoxia. The onset of low oxygen conditions is known to determine broad reconfigurations in plant transcriptomes (28, 29), however the information about the promptness of these responses is scant. To tackle the earliest events of hypoxic signaling, we exposed fully aerated *A. thaliana* seedlings to acute low oxygen (1% O_2 atmosphere) and monitored the expression of hypoxia markers in the first minutes of stress (5', 10', 15'), as well as after more prolonged treatment (1 h, 2 h). Transcripts of all nine hypoxia-responsive genes (HRGs) we selected (24) increased significantly above aerobic levels within 5 to 10 min and kept accumulating over the treatment, following logistic curves (Fig. 1*A* and *SI Appendix*, Table S1). To quantify the speed of activation of each HRG, we used the response time (RT), or the time required to increase mRNA levels from 10% to 90%. *HRA1* (*Hypoxic Response Attenuator 1*) and *LBD41* (*Lateral organ Binding Domain 41*) transcripts increased most rapidly. Two other genes also involved in hypoxia signaling, *PCO1* (*Plant Cysteine Oxidase 1*) and *HRE2* (*Hypoxia Responsive ERF 2*), had intermediate speed of induction, while the rest of the markers, including the hypoxic metabolism landmarks *PDC1* (*Pyruvate Decarboxylase 1*), *ADH1* (*Alcohol Dehydrogenase 1*), and *PGB1* (*Phytoglobin 1*), increased more progressively (Fig. 1*A*).

To understand the contribution of the ERFVII factors to HRG fast activation, we looked at the distribution of hypoxia-responsive promoter elements (HRPE), the ERFVII cognate *cis*-motif (30), in their upstream regions (Fig. 1*A*). Using a linear mixed-effects model (*SI Appendix*), HRPE motif density in HRG promoters was strongly negatively associated with RT (β_1 = −12.4 min per motif/kb; SE = 2.69 min per motif/kb; P = 0.0037), indicating faster responses at higher HRPE density (Fig. 1*B*). The scaled promoter length showed a modest negative association (β_1 = −13.82 min; SE = 5.48 min; P = 0.045) while the intercept was β_1 = 94.93 min (SE = 9.40 min; $P = 5.48 \times 10^{-5}$). Genes with faster response also showcased more concentrated HRPE sequences (Fig. 1*A*). To further assess the relative contributions of HRPE density and promoter length to the RT, we applied a dominance analysis (31, 32) using a linear model that included HRPE density and promoter length as predictors. This analysis showed that HRPE density accounted for the majority of the explained variance in RT (general dominance contribution to R^2 = 0.594, corresponding to approximately 84% of the explained variance), whereas promoter length contributed less (general dominance = 0.114; total $R^2 \approx 0.71$) (*SI Appendix*, Fig. S2*A*). Inspection of residual diagnostics did not reveal strong violations of linear model assumptions (*SI Appendix*, Fig. S2 *B–E*), and gene-level influence diagnostics indicated that the fitted relationship was not driven by a single observation (*SI Appendix*, Fig. S2*F* and Table S2).

In the pentuple *erfVII* mutant (33), the immediate induction of all markers was abolished (Fig. 1*C* and *SI Appendix*, Fig. S3), indicating that no other factor could replace the ERFVIIs as trigger of hypoxic gene activation. At later time points, a partial response was slowly mounted by the *erfVII*. This observation is compatible with the previous report of residual *ERFVII* expression (34).

We monitored ERFVII protein dynamics in early hypoxia, taking advantage of transgenic plants that express the ERFVII RELATED TO APETALA2 3 (RAP2.3) tagged at the C-terminus with a triple HA epitope (35). The extent of posttranslational regulation we observed was comparable with existing reports (5, 35). Proteasome inhibition with bortezomib (BZ) led to strong RAP2.3 accumulation, while hypoxia had a milder effect (Fig. 2 *A* and *B* and *SI Appendix*, Fig. S4*A*). This could be due to a repression of translation (36), or to alternative mechanisms that concur to ERFVII degradation when the Cys-NDP is inhibited, as reported in the *prt6* mutant before (5). Closer inspection revealed that $RAP2.3^{3xHA}$ stabilization occurred as early as 5 min into hypoxia and further protein accumulation was visible until 30 min, after which similar levels were maintained over 8 h treatment (Fig. 2 *C* and *D* and *SI Appendix*, Fig. S4*B*). In contrast with RAP2.3, a direct target of O_2-dependent proteolysis, the hypoxia-inducible proteins ADH and PDC showed a delayed accumulation in hypoxia (*SI Appendix*, Fig. S4*C*). These data overall support the conclusion that $RAP2.3^{3xHA}$ stabilization by hypoxia occurs before the induction of HRGs in Arabidopsis seedlings.

A Plant-Inspired Switch Induces Gene Expression Under Hypoxia in Baker's Yeast. The previous data suggest that ERFVII enrollment and stabilization enables seedlings to perceive and react to sudden hypoxia, activating the transcriptional response. We hereby propose that the inhibition of the proteolytic Cys-NDP pathway can be the all-sufficient cause for the immediate onset of hypoxic transcription. To challenge our hypothesis, we

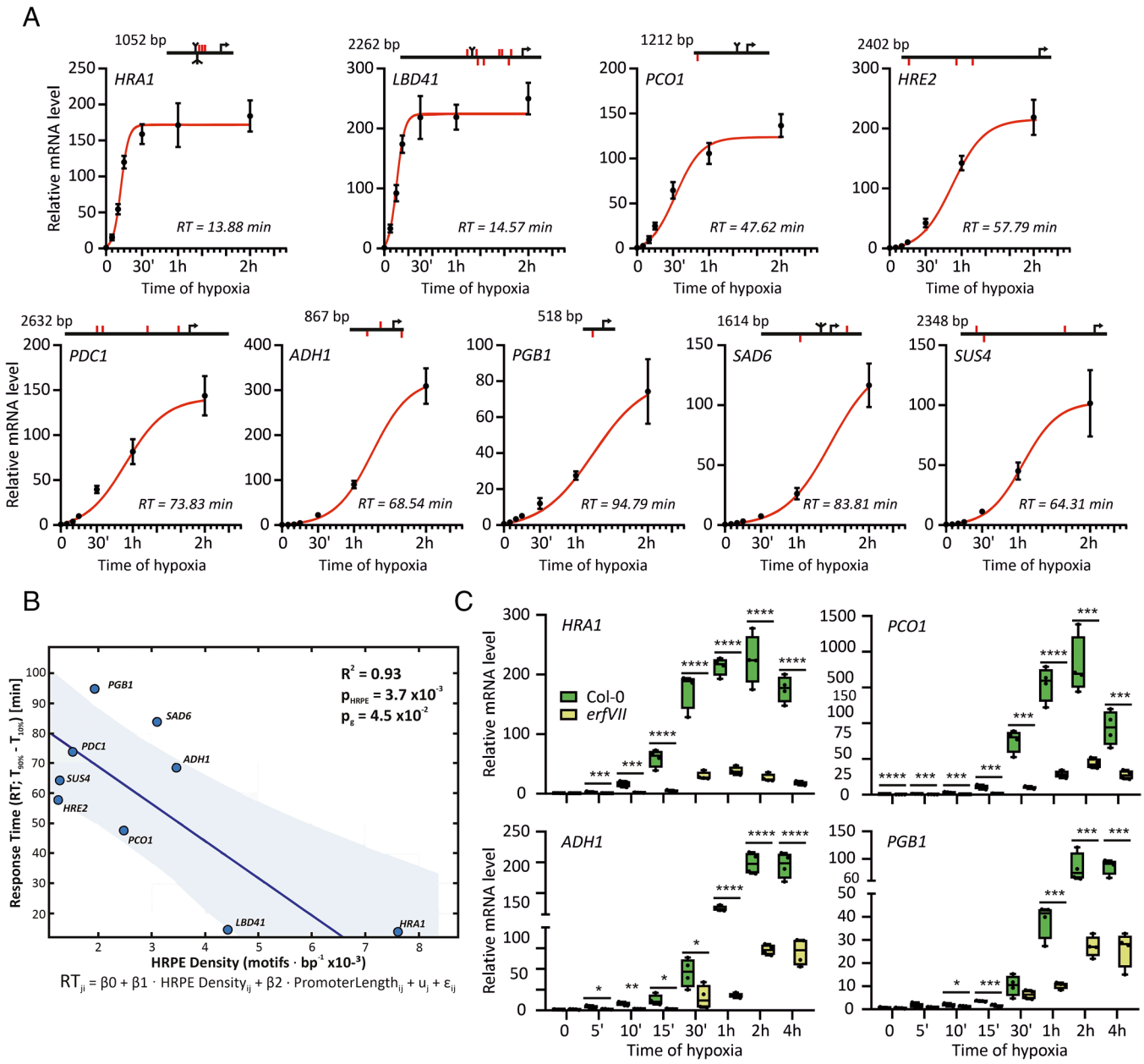

Fig. 1. Short-term profiling of HRG expression in *Arabidopsis thaliana* seedlings. (*A*) Time-resolved expression of nine hypoxia responsive genes: *Hypoxic Response Attenuator 1* (*HRA1*), *Lateral organ Binding Domain 41* (*LBD41*), *Plant Cysteine Oxidase 1* (*PCO1*), *Hypoxia Responsive ERF 2* (*HRE2*), *Pyruvate Decarboxylase 1* (*PDC1*), *Alcohol Dehydrogenase 1* (*ADH1*), *Phytoglobin 1* (*PGB1*), *Stearoyl-Acyl Carrier Protein 6* (*SAD6*) and *Sucrose Synthase 4* (*SUS4*) in 7-d-old Col-0 seedlings growing on vertical plates moved from normoxia (t_0) to hypoxia (1% O_2 v/v) for 2 h. Data are mean ± SD (n = 4). Red lines represent logistic regression fitted to the average expression data at each time-point (*SI Appendix*, Table S1). RT, response time. Above, architecture of the same genetic loci, spanning from up to 2 kb upstream of the ATG codon (arrow) down to the first intron of the gene. Individual HRPEs are highlighted in red, while bi- or tridents indicate 2 or 3 overlapping motifs, respectively. HRPE orientation is also displayed with marks above (presence in the sense DNA strand) or below the horizontal line (presence in antisense strand). (*B*) Correlation between response time (RT) and HRPE density (motifs bp^{-1}) in the HRGs from (*A*). Equation below (see *SI Appendix*, *Extended Methods* for details on the linear model). (*C*) Expression of selected markers in Col-0 and *erfVII* mutant seedlings undergoing an extended 4 h hypoxic treatment, similar to (*A*). Statistically significant differences between Col0 and *erfVII* after Student's *t* test are indicated by asterisks (*0.01 ≤ *P* < 0.05, **0.001 ≤ *P* < 0.01, ***0.0001 ≤ *P* < 0.001, ****P < 0.0001; n = 4).

decided to insulate the Cys-NDP from plant cells and test the dynamics of the hypoxic response into an orthogonal biological system (*S. cerevisiae*). Our plant-inspired circuit for hypoxia-controlled transcription consists of the Cys-NDP reduced to its essential components: a PCO sensor, an ERFVII effector and a *promoter:luciferase* reporter module. The combination of these three modules was expected to generate minimal crosstalk with endogenous regulatory pathways.

Nanoluciferase (NLUC) was chosen for the reporter module, by virtue of its intense signal and fast turnover (37). To confer full orthogonality to the circuit, we adopted a synthetic promoter made of tandem repetitions of the conserved 30-bp HRPE *cis*-element (30, 38). We tested three hypoxia-responsive HRPE promoter versions (HRPE, $HRPE_{ADH}$, and $HRPE_{\Omega}$) that differ in their 5' untranslated region (39). Once integrated in the TRP locus of the yeast strain W303, the promoters showed different levels of basal expression (*SI Appendix*, Fig. S5*A*). HRPE- and $HRPE_{\Omega}$-NLUC produced respectively 10- or 60-fold higher signal than a FLUC normalizing construct, integrated in the HIS3 locus and driven by the constitutive P*GPD* promoter from *glyceraldehyde*

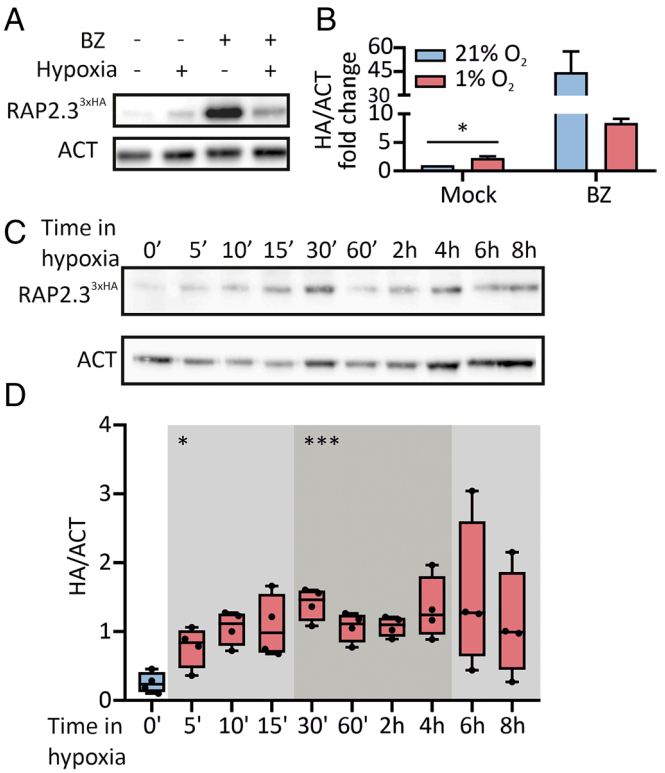

Fig. 2. ERFVII protein regulation in short-term hypoxia. (*A*) Detection of RAP2.3^{3xHA} (HA) and actin (ACT) in liquid grown *35S:RAP2.3^{3xHA}* seedlings, after 6 h treatment with normoxia, 1% O_2, 100 μM bortezomib (BZ), or an equal amount of DMSO (1% v/v, mock). (*B*) Densitometric quantification of RAP2.3^{3xHA} band intensity from the previous blots, normalized to actin (mean + SD, n = 2). Data are expressed as fold change from the mean normoxic mock value. (*C*) RAP2.3^{3xHA} and actin abundance in 7-d-old seedlings from vertical plates, over a time-course of hypoxia extended up to 8 h. (*D*) Quantification of RAP2.3^{3xHA} band intensity (HA/ACT signal ratio), performed as in (*B*). Full blots are provided in *SI Appendix*, Fig. S4. Asterisks in (*B*) indicate statistically significant differences after Student's *t* test (*0.01 ≤ *P* < 0.05; n = 4), shadings and asterisks in (*D*) represent statistically significant differences from normoxia from normoxia (T_0), for One-way Anova (*0.01 ≤ *P* < 0.05, ***0.0001 ≤ *P* < 0.001; n = 4).

3-phosphate dehydrogenase. In contrast, $HRPE_{ADH}$-NLUC produced a low basal output, displaying a desirable feature for inducible systems.

We used the ERFVII protein RAP2.12 from Arabidopsis to design the effector module. The plant TF alone proved unable to activate any HRPE reporter (Fig. 3*A*). We thus tested RAP2.12 C-terminal fusion with three distinct transcription activation domains (TAD): the native yeast GAL4 AD and two synthetic TADs, 6TAL-VP64 and GAL4STE12 (*SI Appendix*, *Extended Methods*). We hereby obtained the synthetic TFs RAP2.12-GAL4AD, RAP2.12-6TVP, and SYRAP (RAP2.12-GAL4STE12, or Synthetic Yeast RAP). Moreover, fusion of SYRAP with an N-terminal ubiquitin monomer generated UbSYRAP (*SI Appendix*, *Extended Methods*). This TF exposes an N-terminal Cys residue upon ubiquitin-mediated protein cleavage, a technique exploited before on a model Cys-NDP substrate in yeast (27).

SYRAP and UbSYRAP outperformed the other two chimeric TFs. GAL4 AD and 6TAL-VP64 domains were not effective when fused with RAP2.12 (Fig. 3*A*). Failure of the first domain may have arisen from a GAL80-mediated repression of GAL4 (40) in place in W303 cells (41). In contrast, SYRAP and UbSYRAP activated *HRPE-NLUC* and $HRPE_{ADH}$-*NLUC*, causing four- to sixfold NLUC enhancement over their GAL4STE12 control (Fig. 3*A*). A similar trend was also visible with $HRPE_{\Omega}$–*NLUC*, although masked by the variability of this highly active promoter.

A preliminary test of the oxygen sensitivity of the two SYRAP versions was made in Arabidopsis, where the Cys-NDP regulation exists natively. Transient transformation of plants expressing a stable $HRPE_{ADH}$-*NLUC* reporter (42) showed that both TFs retained O_2-dependent regulation (Fig. 3*B*). Their strong constitutive expression boosted reporter activity far beyond the levels allowed by the native ERFVII machinery.

Finally, we implemented the O_2-dependent regulation in the yeast circuit with a plant-derived PCO4 module. This modification is in fact known to enable a synthetic Cys-NDP in *S. cerevisiae* (27). Preliminarily, we made sure that a nuclear-localized PCO4 construct was able to process the model substrate DLOR (27) (*SI Appendix*, Fig. S5*B*). We then opted to assess the performance of the circuit in different ranges of output activation; based on the previous results, we thus tested SYRAP and UbSYRAP susceptibility to PCO when combined to *HRPE-* or $HRPE_{ADH}$-*NLUC* modules (Fig. 3*C*). Both PCO4 and normoxia were required to prevent the activation of the promoters, but the regulation was partially masked in the high output range associated with *HRPE-NLUC*. The best regulatory range was attained by combination of UbSYRAP with $HRPE_{ADH}$-*NLUC*, where low output was associated with effective PCO4- and O_2-dependent degradation of the TF (Fig. 3 *D* and *E* and *SI Appendix*, Fig. S5*C*). We thereby demonstrated that a minimal set of plant-derived modules is sufficient to install O_2-dependent transcriptional circuits in *S. cerevisiae*.

Relying on the dual DNA binding capacity of SYRAP effectors, we explored the possibility to associate this synthetic regulation with UAS_{GAL} promoters (Fig. 3*F*). To this end, we deployed two UAS_{GAL} genomic insertions, P*HIS3*UAS_{GAL1}-*HIS3* and P*GAL1-LACZ*, carried by the MaV203 strain (41). Aerobic growth of cultures expressing either SYRAP or UbSYRAP on selective histidine-deficient media was indeed PCO4-dependent (*SI Appendix*, Fig. S6 *A* and *B*). The β-galactosidase assay confirmed strong aerobic activation of *LACZ* by the two SYRAPs, activation prevented if PCO4 was expressed (*SI Appendix*, Fig. S6*C*). Also on solid media, SYRAP and UbSYRAP colonies showed PCO4-mediated growth repression in aerobic conditions (*SI Appendix*, Fig. S6*D*). As expected, PCO4-positive UbSYRAP colonies developing in hypoxia were instead undistinguishable from PCO4-negative colonies (Fig. 3*G*). These experiments suggest that ERFVII-based transcriptional circuits represent a viable strategy to achieve O_2-dependent control of complex responses, such as growth, in yeast without interference with the endogenous O_2 signaling pathways (*i.e.,* orthogonally).

Fast and Reversible Responses to O_2 Variations are Produced by the Minimal ERFVII-Based Transcriptional Circuit. The assembly of PCO4, UbSYRAP, and $HRPE_{ADH}$-*NLUC* modules was adopted for subsequent experiments and designated as MynOx, for Minimal yeast Oxygen-responsive circuit (Fig. 3*F*). MynOx yeast was meant to serve as a heterologous model for plant hypoxic regulation; a precondition to its use was thus to ensure that yeast cells could be exposed to low oxygen in a way that faithfully approximated the conditions experienced by seedlings in Fig. 1*A*.

We initially monitored MynOx output in hypoxic liquid cultures, while recording O_2 concentration in the medium with a sensor spot, as described in (43). O_2 depletion was associated with progressive output increase (Fig. 4*A*), as expected only in presence of PCO4. The treatment was protracted until the cultures reached complete anoxia, after which they were reoxygenated. By the time dissolved O_2 was restored to prehypoxic levels, the NLUC output had fallen from fourfold induction to twofold the initial aerobic values (Fig. 4*A*), indicating that MynOx generates quantitative and reversible responses to O_2 fluctuations. However, the culture

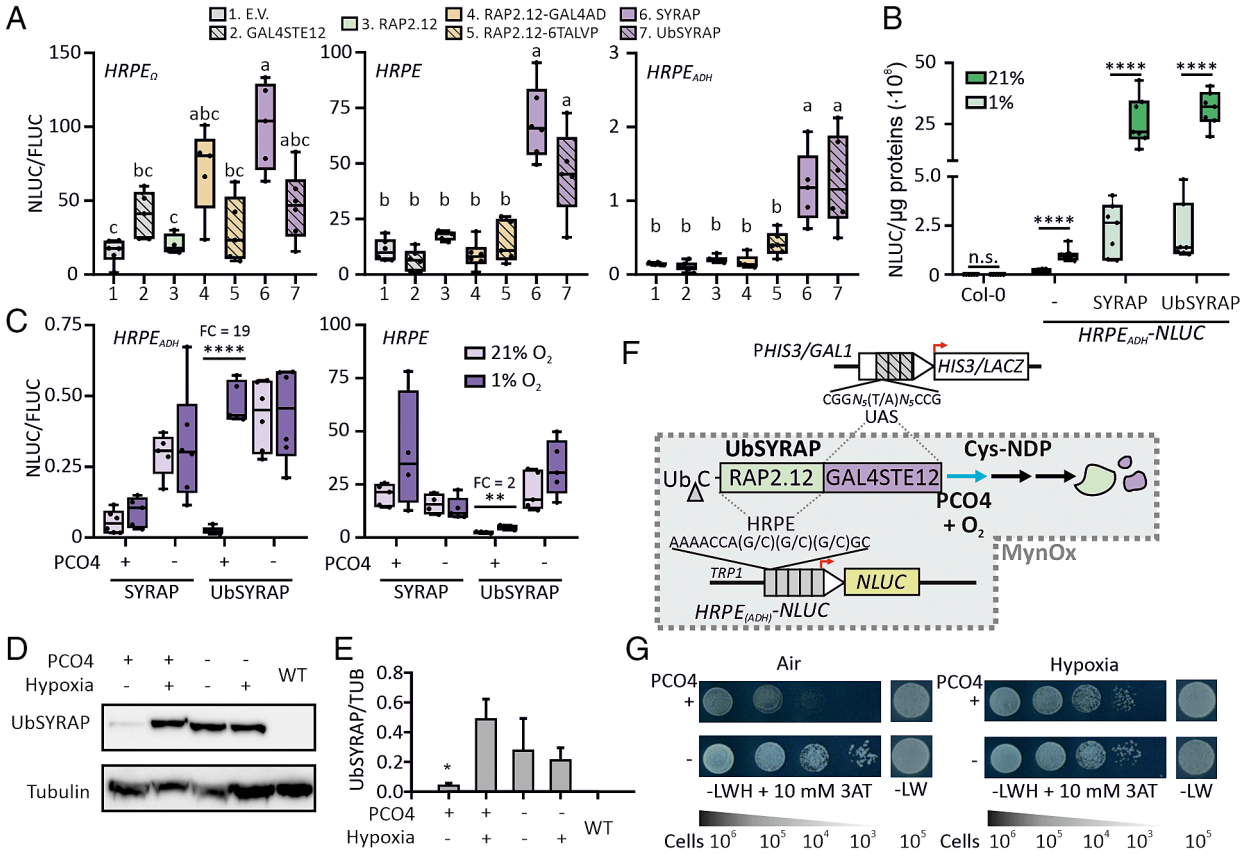

Fig. 3. Assembly of orthogonal ERFVII-based transcriptional circuits in yeast. (*A*) Activation of three synthetic promoter versions (*HRPE-, HRPE$_{ADH}$-, and HRPE$_{\Omega}$-NLUC*) by RAP2.12-derived TFs in W303 cultures. Cells were cotransformed with a P*GPD-FLUC* integrative construct and HRPE promoter activity was expressed as relative NLUC activity (NLUC/FLUC) (n = 5 to 6). E.V., empty vector. (*B*) Transient expression of *35S:SYRAP* constructs in agroinfiltrated leaves of Arabidopsis plants. The activity of an *HRPE$_{ADH}$-NLUC* reporter, stably integrated in the genome, was recorded after 6 h incubation in normoxia or hypoxia (n = 6). Water-infiltrated leaves from the wild type ("Col-0") or *HRPE$_{ADH}$-NLUC* ("-") were included. (*C*) O_2-dependent regulation of *HRPE-* and *HRPE$_{ADH}$-NLUC* reporters in W303 yeast expressing SYRAP or UbSYRAP along with PCO4 or a control protein (GUS, −). Cultures (n = 4 to 5) were incubated for 6 h in normoxia or hypoxia (1% O_2). NLUC activity was normalized to P*GPD-FLUC* activity. Fold changes values (hypoxia vs. air; FC) are reported above the significantly different groups. (*D*) Regulation of UbSYRAP protein abundance, detected with an anti-GAL4BD antibody, by PCO4 and hypoxia (6 h, 1% O_2). WT, aerobic untransformed cells. (*E*) Relative UbSYRAP amount to α-tubulin (mean + SD, n = 3), quantified by densitometry from blots in *SI Appendix*, Fig. S5*C*. (*F*) Schematic overview of the synthetic O_2-responsive circuits. The RAP2.12- and GAL4-derived DNA binding domains of UbSYRAP make the chimeric TF able to recognize both HRPE and UAS_{GAL} elements. UbSYRAP acts as effector of *NLUC* expression in W303 strains, or *HIS3* and *LACZ* expression in MaV203 strains. O_2 enables UbSYRAP degradation through PCO4, thereby lowering the output(s). The wedge indicates ubiquitin (Ub) cleavage by yeast deubiquitinases. (*G*) Growth of MaV203 cells expressing UbSYRAP in combination with PCO4 (+) or GUS (−), after 3 d incubation in normoxia or hypoxia. SD–LW, nonselective medium; SD–LWH, selective medium, supplemented with 10 mM 3-AT. The approximate number of cells spotted is reported below. Different letters in (*A*) or asterisks in (*E*) indicate statistically significant differences ($P < 0.05$) after One-way Anova; asterisks in (*B* and *C*) indicate statistically significant differences after Student's *t* test on pairwise comparisons (*$0.01 \le P < 0.05$, **$0.001 \le P < 0.01$, ****$P < 0.0001$).

medium underwent slow equilibration with the hypoxic atmosphere, which associated with a gradual and linear increase of the output. In this set-up, failure to maintain a steady-state level of dissolved O_2, likely due to fast consumption by proliferating cells, precluded the possibility to titrate MynOx output as a function of O_2 concentration. To overcome these limitations, we applied a different treatment set-up, resuspending the cultures in media that had been pre-equilibrated under hypoxia. This time, stationary O_2 levels could be maintained for at least 1 h, enabling a time-resolved analysis of the response (or "hypoxic chase", Fig. 4*B*). Cultures equilibrated at 1% O_2 quickly reached a plateau of NLUC signal in 10 min, whereas no response was observed in cultures exposed to very mild hypoxia (10% O_2) (Fig. 4*B*). We concluded that MynOx could react promptly to acute hypoxia, depending on the perceived level of oxygen in cells.

These observations directed us to shift from liquid cultures to thin-layered colonies, whose morphology should prevent the formation of oxygen gradients. Cells in such colonies were expected to remain equilibrated with the atmosphere for longer time than cultures and better approximate the speculated situation in seedling tissues. We thus compared the dynamic output of MynOx colonies with *HRPE$_{ADH}$-NLUC* Arabidopsis seedlings, over a timing of hypoxia. *NLUC* mRNA built up quickly both in plants (Fig. 4*C* and *SI Appendix*, Fig. S7*A*) and yeast (Fig. 4*E*). Remarkably, the rate of *NLUC* accumulation was the same as the *ADH1* transcript (*SI Appendix*, Figs. S5*C* and S7*A*), suggesting that the synthetic HRPE promoter could recapitulate the dynamics of endogenous genes and pointing at a decisive role for the 5'-UTR in *ADH1* regulation. The NLUC output showed sizable delay in plants (Fig. 4*D* and *SI Appendix* Fig. S7*B*), whereas it closely followed mRNA pattern in yeast (Fig. 4*F*). The lag in plants may be explained due to selective protein translation (44), in contrast with hypoxic promotion of protein synthesis in yeast (45, 46).

After the initial induction, nonetheless, the responses diverged with time. *NLUC* mRNA kept accumulating until the end of a 2 h-long treatment in seedlings (Fig. 4*C*), while in yeast it reached a steady-state within few minutes (Fig. 4*E*). Moreover, the response range was incomparably smaller in MynOx than Arabidopsis (2.5-fold *NLUC* induction in yeast, 200-fold in seedlings). These data highlight that the minimal circuit, although able to trigger

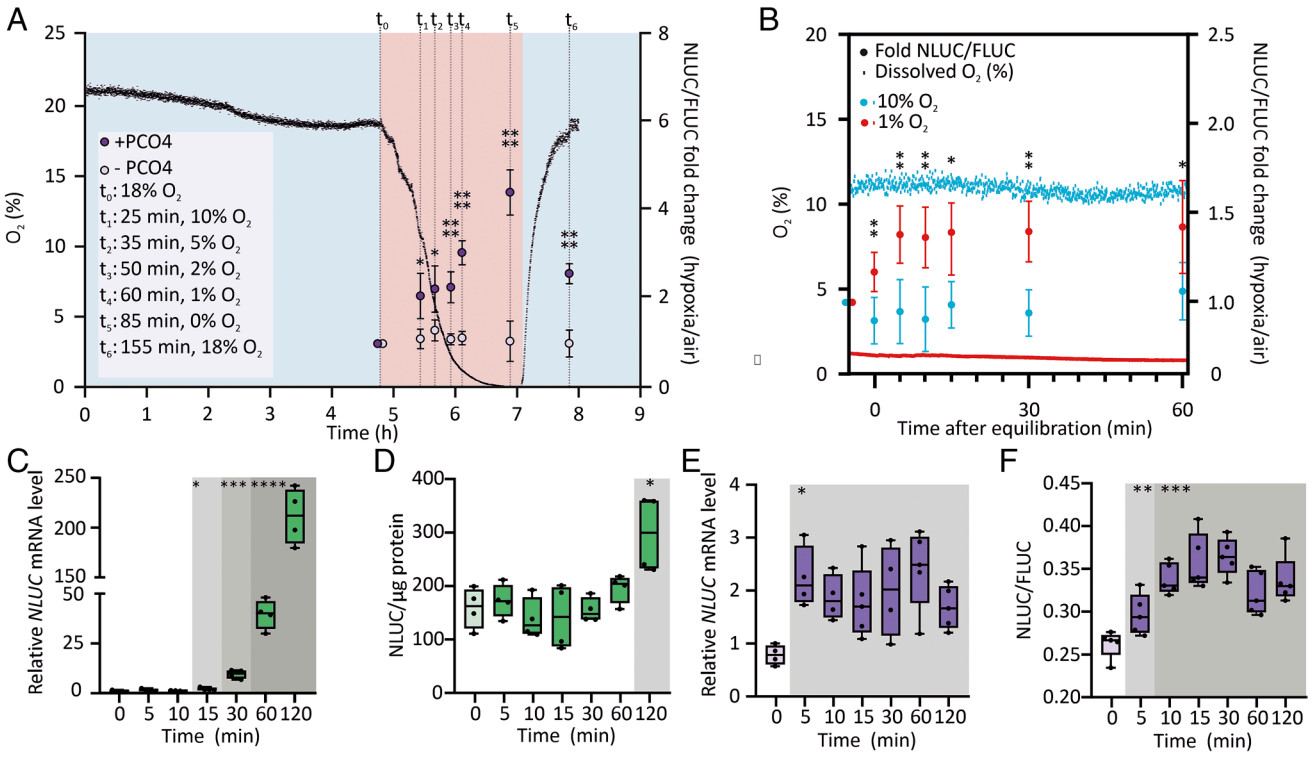

Fig. 4. Recapitulation of plant hypoxic dynamics in yeast. (*A*) Evolution of *HRPE$_{ADH}$-NLUC* output in cells expressing PCO4 (purple dots) or GUS (yellow dots). Cultures grown for 5 h in normoxia (t_0 of the treatment) were maintained in a 1% O_2 hypoxic atmosphere (red shading). Reoxygenation (blue shading) was applied after anoxia was reached in a reference culture, where dissolved O_2 levels were monitored (black profile), and was protracted until O_2 reached back the t_0 level (18%, v/v). Data are expressed as fold changes of NLUC/FLUC activity between hypoxic and normoxic (t_0) samples (mean ± SD, n = 5). (*B*) Output of MynOx cultures in "hypoxic chase" experiments. Cultures grown for 5 h in normoxia were resuspended in media equilibrated at 10% (blue) or 1% O_2 (red) and incubated under the corresponding hypoxic atmosphere. NLUC activity (dots) was monitored at 5, 10, 15, 20, 30, and 60 min after culture equilibration with the hypoxic media and expressed as fold change of NLUC/FLUC activity over normoxia (mean ± SD, n = 5). Colored profiles show O_2 concentration (% v/v) in the culture. (*C*) *NLUC* expression in 7-d-old *HRPE$_{ADH}$:NLUC* seedlings from vertical plates, normalized to the *UBQ10* housekeeping gene and made relative to a t_0 sample (n = 4). (*D*) Relative NLUC activity in the same seedlings. (*E*) *NLUC* expression in MynOx thin colonies, normalized to *Actin 1* and made relative to a t_0 sample (n = 4 to 5). (*F*) NLUC/FLUC activity in the same colonies. Asterisks indicate significant differences (*$0.01 \le P < 0.05$, **$0.001 \le P < 0.01$, ***$0.0001 \le P < 0.001$, ****$P < 0.0001$) after Student's *t* test on pairwise comparisons between + and -PCO4 (*A*), 1% and 10% O_2 (*B*), or after multiple *t* test between each timepoint and t_0 (normoxia, *C*–*F*).

HRPE$_{ADH}$-NLUC expression, was insufficient to establish a complete transcriptional response in yeast.

Sustained Induction of Anaerobic Gene Expression Requires Positive ERFVII-Regulated Feedback. A major difference between the two *HRPE*-inducing devices compared above resided in the fact that plants incorporate a hypoxia- and ERFVII-regulated feedback loop. In Arabidopsis, constitutively expressed ERFVII paralogs (AtRAP2.2/3/12) are initially stabilized under low oxygen, upon inhibition of constitutively expressed PCOs (AtPCO3/4/5), and in turn trigger the expression of hypoxia-inducible *ERFVII* (*AtHRE1/2*) and *PCO* (*AtPCO1/2*) genes (7, 47). To estimate the impact of this feedback in the plant hypoxic response, we introduced it into MynOx. We transformed *MATα* W303 cells with two ERFVII-inducible modules, HRPE$_{ADH}$-UbSYRAP (U) and HRPE$_{ADH}$-PCO1 (P), or their respective HRPE$_{ADH}$-GUS control constructs (G). Mating of each *MATα* strain with MynOx (*MATa*) wired the inducible modules to the existing minimal circuit (Fig. 5*A*). The four diploid strains obtained, designated by their *MATα*-specific genotype hereafter, contained no new inducible module (GG), HRPE$_{ADH}$-UbSYRAP only (UG), HRPE$_{ADH}$-PCO1 only (GP), or both HRPE$_{ADH}$-UbSYRAP and HRPE$_{ADH}$-PCO1 (UP). After 6 h hypoxia, control diploid cultures (GG) reached comparable output to the parental haploid strain (Figs. 3*C* and 5*B*), whereas the hypoxic output expanded significantly by addition of the HRPE$_{ADH}$-UbSYRAP module (UP and UG) (Fig. 5*B*). A chimeric factor derived from AtHRE2 (HRPE$_{ADH}$-UbSYHRE), unable to bind the HRPE directly (30), left the minimal output unchanged (*SI Appendix*, Fig. S8 *A* and *B*). Finally, addition of HRPE$_{ADH}$-PCO1 alone (GP) produced negligible effects (Fig. 5*B*).

We then profiled the response of diploid genotypes to steady-state hypoxia in a time-resolved experiment (Fig. 5*C*). The induction in the absence of feedback was fast but contained (GG), with similar range to the haploid MynOx (Fig. 4*F*). Introduction of the inducible PCO1 module (GP) did not alter circuit behavior. The inducible TF alone (UG) increased NLUC induction to threefold but could not prolong the response beyond 10 min treatment. With the full feedback (UP), instead, the initial induction was maintained and the time of response stretched, at a nonlinear rate, up to 2 h into the treatment (Fig. 5*C*). As a result, UP enhanced the 1.5-fold dynamic range of GG at 4 h to fivefold (Fig. 5*C*). The UbSYRAP protein accumulated to higher levels in UG and UP under hypoxia than in other genotypes (Fig. 5 *D* and *E* and *SI Appendix*, Figs. S8 *C* and *D* and S9), supported by higher *UbSYRAP* expression (*SI Appendix*, Fig. S8*E*), and *NLUC* expression increased by around fourfolds in steady-state conditions (Fig. 5*F*). Early hypoxia (5') induced *NLUC* in all genotypes except for GP (*SI Appendix*, Fig. S10), but *NLUC* expression could be maintained over a 4-h time-course only when the inducible UbSYRAP module was present, in UP and UG, while the expression declined in GG and GP. The differences among genotypes were not associated with general alterations in endogenous transcription, as shown by use of yeast anaerobic gene markers (*SI Appendix*, Fig. S8*F*), indicating that the synthetic circuit acted

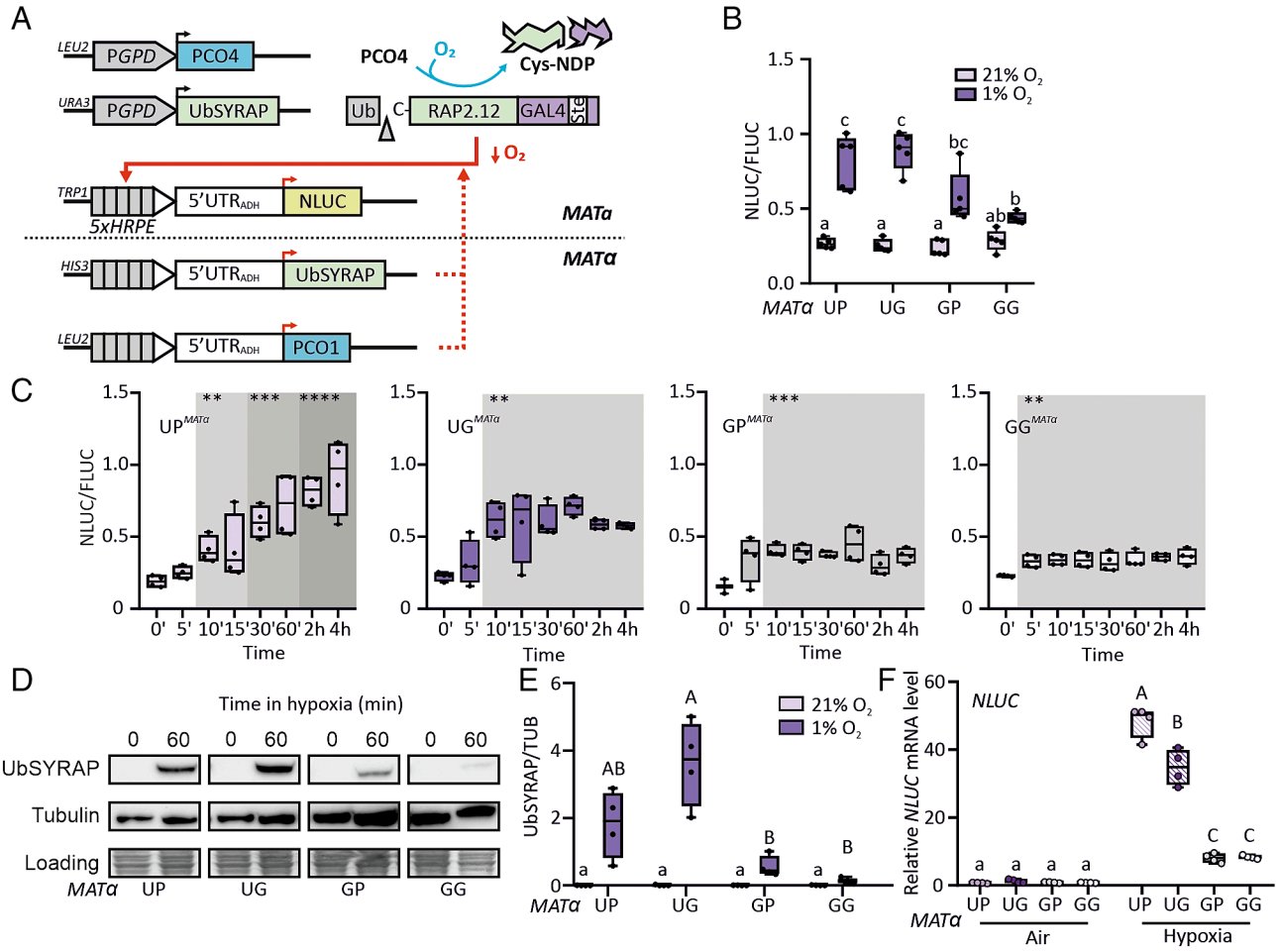

Fig. 5. Introduction of a positive hypoxia-responsive feedback circuit in yeast. (*A*) Schematics of the modules expressed in the diploid W303 strain. The ERFVII-inducible modules $HRPE_{ADH}$-UbSYRAP and $HRPE_{ADH}$-PCO1 were introduced in *MATα* cells, to be combined with the constitutive modules from $MynOx^{MATα}$, controlled by glyceraldehyde 3-phosphate promoters (*PGPD*). Hypoxia triggers positive feedback through activation of the inducible modules. (*B*) Relative NLUC activity (NLUC/FLUC; n = 5) in diploid cultures after 6 h hypoxic (red boxes) or aerobic treatment (blue boxes). The *MATα* genotypes mated with $MynOx^{MATα}$ consisted of combinations of $HRPE_{ADH}$-UbSYRAP (U), $HRPE_{ADH}$-PCO1 (P), or $HRPE_{ADH}$-GUS (G, negative control) modules, integrated either at the *HIS3* or *LEU2* locus. (*C*) Evolution of NLUC activity (n = 4) in diploid colonies moved from normoxia (t_0) to 4 h-long hypoxia (1% O_2). (*D*) UbSYRAP protein abundance in normoxic diploid cultures (t_0) or after 1 h incubation in hypoxia in pre-equilibrated medium. (*E*) Normalized band intensity to α-tubulin, in independent biological replicates (n = 4). (*F*) *NLUC* mRNA abundance, normalized on *ACT1* expression, in different diploid cultures treated as in (*D*). Data are relative to an aerobic $GP^{MATα}$ sample. Asterisks and shadings indicate significant differences (**0.001 ≤ *P* < 0.01, ***0.0001 ≤ *P* < 0.001, ****P < 0.0001) after multiple Student's *t* tests between each time point in hypoxia and t_0. Different letters in (*E* and *F*) indicate statistically significant differences among normoxic (*Lowercase*) or hypoxic samples (*Uppercase*), after One-way Anova, while in (*B*), they indicate differences between groups and treatments after Two-way Anova was performed (P < 0.05).

orthogonally to yeast anaerobic pathways. In pre-equilibrated cultures, UbSYRAP abundance increased faster and to slightly higher levels in UG (*SI Appendix*, Fig. S8D); despite this, we observed higher *NLUC* expression in UP after 1 h hypoxia (Fig. 5*F*).

Although we cannot rule out the existence of indirect effects of PCO1 expression improving *NLUC* mRNA processing or translation, the previous data suggest that combination of a hypoxia-inducible ERFVII module with an inducible PCO1 module was sufficient to expand the time of response and dynamic range of the output. Altogether, by implementing basic ERFVII-regulated feedback in our simplified circuit in a yeast model, we could conclude that constitutively expressed RAP2-type *ERFVII*s are responsible and sufficient for the immediate activation of target genes, but a low oxygen-inducible ERFVII/PCO feedback mechanism is required to prevent a fast decline of the response and support higher induction rates.

Mathematical Modeling Reveals Key Circuit Features to Achieve Fast Transcriptional Responses to Hypoxia. We constructed four mathematical models, backed up by the output data collected, to interpret the behavior of the diploid strains. The models ranged in complexity from the essential circuit based on a single ERFVII and a PCO4 (GG), to the simplified feedback loop including hypoxia-inducible copies of both modules (Fig. 6*A*). The coupled Ordinary Differential Equations (ODEs) defining every model (*SI Appendix*, Table S3) were built using the reaction rates reported in *SI Appendix*, Table S4. The kinetic variables for Cys2 oxidation by PCO4 and PCO1, the only oxygen rate-limited step in the pathway, were refitted from in vitro data (12) (SI Appendix, Fig. S11*A*). The rates of UbSYRAP synthesis and degradation (k1 and k2, *SI Appendix*, Table S5) were calculated from our previous assessment of $RAP2.12_{2-50}$ stability from the model substrate DLOR, in yeast cultures treated under similar hypoxic conditions as here (27) (SI Appendix, Fig. S11*B*). All other parameters of the models were calculated to best fit our experimental data (*SI Appendix*, Table S5). The obtained simulations compared well with the experimental NLUC induction (NLUC/FLUC; Figs. 5*C* and 6*B*) indicating that the nonlinear fitting was accurate, and the parameters reasonable (*SI Appendix*, Table S7). Compatible with the experimental observations, UbSYRAP amount decreased

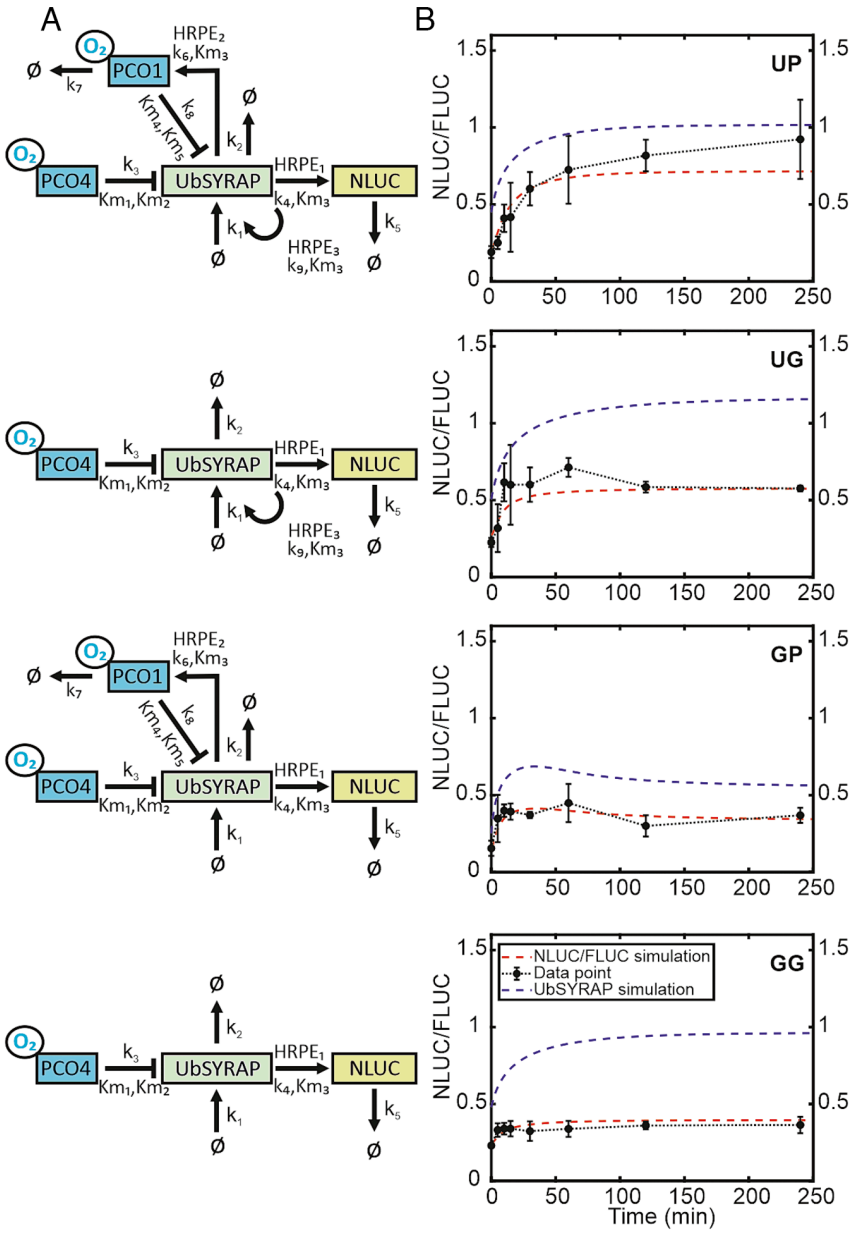

Fig. 6. Mathematical modeling of the synthetic O_2-responsive circuit of yeast. (*A*) Schematic architecture of the models corresponding to the four genetic circuits illustrated in Fig. 5. All species included in the models (UbSYRAP, PCO1/4, O_2, and NLUC, output corresponding to the NLUC/FLUC output in yeast) are framed, while the "Ø" symbol stands for "null." (*B*) Computational simulation of NLUC activity based on the respective model architectures presented in (*A*) (red line), overlapped with the experimental data from Fig. 5C (NLUC/FLUC, black line). The adjusted UbSYRAP concentration (blue line, "UbSYRAP simulation") was obtained from the steady-state simulations, fitted as described in the *SI Appendix, Extended Methods* and shown in *SI Appendix*, Fig. S11 (27).

over time in GP, but not in UP (Fig. 6*B*), suggesting that the hypoxia-inducible PCO1 retains activity under 1% O_2 atmosphere, but repression is overcome by the presence of a hypoxia-inducible copy of the TF.

We observed changes in the parameter values across the four models, revealing that the binding rate of UbSYRAP to different HRPE promoters significantly influences system behavior. Notably, the binding rates of UbSYRAP to *HRPE$_{ADH}$-NLUC* ($HRPE_1$, output module) varied among GG, GP, UG, and UP models (0.07, 0.06, 0.04, and 0.02, respectively; *SI Appendix*, Table S5). Introduction of a hypoxia-inducible UbSYRAP copy (*HRPE$_{ADH}$-UbSYRAP*) in UG and UP showed a more substantial $HRPE_1$ reduction than *HRPE$_{ADH}$-PCO1* only (GP). Similarly, the predicted binding rates of UbSYRAP to *HRPE$_{ADH}$-PCO1* ($HRPE_2$) and *HRPE$_{ADH}$-UbSYRAP* ($HRPE_3$) were lower in UP, with both inducible components present. The lowest $HRPE_{1/2/3}$ values in UP (*SI Appendix*, Table S5) suggest a competitive interaction among promoters for UbSYRAP recruitment, leading to further modulation in their individual binding efficiencies.

We examined how the full-feedback model UP, which resembles plant cell regulation most closely, responded to variations of individual parameters (*SI Appendix*, Fig. S10*A*), based on NLUC RT ($t_{90\%}$-$t_{10\%}$, a proxy of NLUC/FLUC induction speed) as model performance metric. Interestingly, among the top-ranking parameters influencing the RT, five were linked to PCO1: k_{6-8} (PCO1 degradation, PCO1 synthesis, and UbSYRAP oxidation rate by PCO1) and Km_{4-5}, accounting for the refitted Michaelis–Menten constants for O_2 and UbSYRAP as PCO1 substrates (*SI Appendix*, Fig. S12 *B* and *C* and Table S4). Overall, high PCO1 activity under hypoxia resulted to be associated with shorter RT. Our analysis puts forward a potential strategy to enhance the speed of plant hypoxic responses through PCO1 engineering, leading to higher affinity for O_2 and RAP2.12 (lower Km_{4-5}), elevated catalytic rate for RAP2.12 oxidation (k_8) or higher PCO1 abundance (higher k_6, or lower k_7) (*SI Appendix*, Fig. S12C).

Discussion

Plant ERFVII TFs have long been identified as responsible to orchestrate the expression of low oxygen-inducible genes in plants (24, 48). The ERFVII proteins are normoxically degraded via the

cysteine- (or PCO-) branch of the N-degron pathway (Cys-NDP) and stabilized when oxygen levels fall (9, 10), which creates a mechanistic link between the ERFVII and the observed responses. However, the expected prompt activation of hypoxia-responsive genes seems to conflict with evidence of ERFVII protein stabilization after longer treatments, collected using fluorescent reporters and immunoblots (18, 35). This has led to speculation that additional mechanisms are needed to generate the first response to hypoxia in plants, potentially acting upstream of the ERFVIIs, or in parallel to them but with faster dynamics (23, 49). Transcriptomic studies have defined the signature of acute hypoxia as early as 30' into the treatment (29, 50), nonetheless quicker induction of transcription has been found with marker genes (30, 51). Here, we showed that anaerobic markers (HRGs) are already upregulated after 5 min exposure of plant tissues to hypoxia (Fig. 1*A*). Importantly, we obtained evidence that correlates the timing of the transcriptional response with increased $RAP2.3^{3xHA}$ protein amount (Fig. 2 *C* and *D*), in support of the hypothesis that signaling events leading to fast ERFVII stabilization are a requisite for HRG induction.

Anaerobic transcription in seedlings was as expected sustained, until at least 4 h treatment (Fig. 1 *A* and *C* and *SI Appendix*, Fig. S7C). Hypoxia causes coordinated epigenetic modifications in up-regulated HRG regions. The chromatin at these loci becomes more accessible early under low oxygen, the repressive H2A.Z histone form is displaced, and transcription is promoted by the rise of activating histone modifications, such as H3K9ac (36, 52). Chromatin remodeling factors are also recruited onto HRG loci through the Mediator complex, after ERFVII binding to their upstream sequences (53–55). In agreement with the role of ERFVIIs in promoting the accessibility of up-regulated genes, we found a correlation between the different profiles of HRG induction and the distribution of HRPE *cis*-motifs bound by RAP-type ERFVIIs (Fig. 1*B*). This suggests that ERFVIIs can determine both the amplitude and speed of the hypoxic responses. The synthetic $HRPE_{ADH}$ promoter showed intermediate RT in plants (like the endogenous gene *ADH1, SI Appendix*, Fig. S7A), despite five tandem repetitions, implying that the exact profile of HRG expression depends on HRPE arrangement. The same promoter construct was quickly induced by hypoxia in yeast but could not reach the induction levels observed in plants (Fig. 5*F* and *SI Appendix*, Fig. S10). Despite conservation of the core chromatin remodeling machinery in yeast (56, 57), inefficient association with ERFVII transcriptional complexes may partially account for these discrepancies in *NLUC* output.

Our main goal was to measure the contribution of ERFVII conditional proteostasis to HRG induction, disentangling it from other cross-regulating signaling events associated with hypoxia in plant cells. Observing the genuine effects of the Cys-NDP on ERFVII activity entails the ability to insulate that pathway from others potentially impinging on the same protein targets. Synthetic biology provides the ideal framework to manage the reduction of complex biological behaviors into simpler functioning schemes (26, 58). Abstraction of signaling elements from the native plant host has been successfully attempted before, facilitated by the intrinsic modularity of signaling mechanisms (59, 60). For instance, engineering of core components of plant nuclear auxin signaling in yeast has unveiled the hierarchical relationships among Aux/IAA factors (61), otherwise masked by genetic redundancy of the pathway, feedback, and cross-regulation. We pursued our goal with a similar strategy, reconstituting an O_2-dependent transcriptional circuit by abstraction of essential modules of the plant Cys-NDP.

The minimal O_2-responsive circuit (MynOx, Fig. 3*F*) demonstrated that coupling of an ERFVII-based effector with a PCO4 sensor was enough to provide hypoxic activation of $HRPE_{ADH.}$ The reliability of a heterologous model of plant oxygen sensing also depends crucially on the possibility to control O_2 supply to cells. We identified thin-layered colonies as the best material to approximate the effects of plant seedling tissues exposure to hypoxia (Fig. 4). The comparable speed of output activation in yeast colonies or Arabidopsis seedlings exposed to the same hypoxic atmosphere (Fig. 4 *C* and *E* and *SI Appendix*, Fig. S7), indicates that the most immediate response in Arabidopsis relies exclusively on PCO-dependent signaling. Recently, fast translocation of the calcium-dependent protein kinase CIPK12 to the nucleus has been suggested to protect the ERFVII factors from degradation during hypoxia in Arabidopsis, potentially providing a stabilization mechanism independent of the Cys-NDP (20). The CIPK12 pathway is unlikely to be conserved in yeast, where hypoxia alone has not been shown to directly trigger calcium signaling (62). Although we cannot exclude phosphorylation of the synthetic RAP2.12, hypoxia could only induce MynOx output (or a growth output) in cells expressing PCO4 (Figs. 3*G* and 4*A*).

The design of MynOx highlighted the importance to adapt the effector module to yeast transcriptional requirements. The plant-native activation domain of RAP2.12 was not functional in yeast (Fig. 3*A* and *SI Appendix*, Fig. S6), nor was the synthetic VP64 domain in our hands (Fig. 3*A*). In the first case, specific mediator complex subunits, absent in *S. cerevisiae*, might be required to recruit the RNA polymerase (60, 63). Domains derived from the herpes simplex virus TF VP16, instead, have shown limitation in yeast before, due to leaky or hyperexpression of the adopted constructs (64). Cognate HRPE promoters were taken from Panicucci et al. (39), with no further adaptation. All sequences contained a −47 to +36 fragment from the 35S promoter of Cauliflower Mosaic virus (65), transcriptionally functional in yeast and presenting a compatible TATA box consensus sequence (66, 67) 31 nt upstream of the TSS. Addition of the omega leader sequence of Tobacco Mosaic Virus (68) caused intense NLUC translation in basal conditions and severely limited the dynamic range of the output; in contrast, the 5'-UTR sequence from Arabidopsis *ADH1* conferred broad dynamic range to MynOx (Fig. 3 *A* and *C* and *SI Appendix*, Fig. S5A). These results highlight the importance of the correct choice of 5'UTR regions for the precision control of yeast genetic circuits (69, 70).

Plant *ERFVII* and *PCO* gene families include hypoxia-inducible members (48, 71). The divergence of hypoxia-inducible (or B-type) *PCOs* is puzzling, but their conservation in Spermatophytes (47) indicates that they are under selective pressure. The limited range of response displayed by MynOx, in contrast with the output of $HRPE_{ADH}$ seedlings (Fig. 4 *C–F* and *SI Appendix*, Fig. S7 *A* and *B*), prompts to speculate that the hypoxia-inducible components of the regulatory mechanism are instrumental to the amplitude of *HRG* response. MynOx expansion by rational design (Fig. 5*A*) in fact improved the output only in presence of both $HRPE_{ADH}$-driven modules (Fig. 5 *C* and *F* and *SI Appendix*, Fig. S10). B-type PCOs have been proposed to optimize ERFVII processing during O_2 fluctuations, however their functions during acute hypoxia could not be disentangled through genetics so far (47). Our data show that B-type PCOs are specifically required to regulate the amplitude and duration of the anaerobic response. PCO1 introduction in the circuit produced sizable effects in 1% O_2 atmosphere, hinting at different kinetic properties of these enzymes in vivo than measured in vitro (12). The fitted model predicted a progressive depletion of the constitutive RAP2.12 pool in GP under hypoxia, resulting in low output (Fig. 5*B*) and low target gene expression (*SI Appendix*, Fig. S10). This outcome matches well with the early decline in *HRG* transcripts observed

in *hre1hre2* mutants (48). Here, lack of inducible *ERFVIIs* able to counteract the B-type PCOs led to plant inability to sustain the anaerobic response. Our heterologous model thus suggests that the coevolution of hypoxia-inducible *PCO* and *ERFVII* genes installed a regulatory loop that shapes plant transcription under stress. The parameter sensitivity analysis further detailed the role for B-type PCOs in hypoxia, specifically at tuning the output speed (*SI Appendix*, Fig. S12). This provides further insight into rational B-type PCO modifications increasing their concentration or affinity toward O_2 and RAP2s, in order to speed up transcriptional responses to hypoxia in plants.

The modular architecture of our heterologous model also enabled us to pinpoint the competition among HRPE-containing promoters during hypoxia. The four fitted models showed that UbSYRAP binding rate to the promoter of the output module ($HRPE_1$) was influenced by the presence of other RAP2.12-inducible modules, assuming its lowest value in the UP model (*SI Appendix*, Table S5). This highlights the critical role of ERFVII binding kinetics in modulating HRG expression dynamics. According to competition theory models, multiple promoters sharing the same *cis*-elements are expected to compete for the recruitment of cognate TFs present in limited pools (72, 73). The theory has found broad implications in molecular contexts (73–75). In the case of coexpression networks coordinated by individual TF families, such as the plant HRG network, competition (also indicated as "TF titration") can explain the diversification of target gene expression patterns (73). According to the regulatory model, titration phenomena can generate nonlinear responses, such as digital outputs as in the winner-take-all (WTA) effect (76), or define the expression hierarchy of the targets (72, 77). The competition phenomenon revealed by our model provides a possible explanation for the expression kinetics observed in Fig. 1, with fast HRG induction being dictated by stronger HRPE arrangements in presence of limited RAP TF pools (compatible with the speculative model suggested by other authors (77)).

By virtue of its modularity, our synthetic yeast model represents an ideal tool to compare the binding affinity of different ERFVIIs to HRPEs and thereby start disentangling the questions related to the functional specificities of RAP2-type paralogs in plants (78, 79), which have remained unaddressed so far. We could confirm that HRE-type ERFVII are unable to associate with HRPE promoter elements (*SI Appendix*, Fig. S8*A*), as reported before by Gasch et al. and Lee and Bailey-Serres (30, 36). This evidence indicates that redesign of the output module by incorporation of GCC-rich motifs (36) should make it possible to implement HRE-based hypoxic feedback in the synthetic model and thereby quantify the share of HRE regulation in the long-term anaerobic output.

In conclusion, in this study, we engineered a "plantified" yeast strain to serve as foundational model of synthetic oxygen-dependent transcriptional devices. We demonstrated that this is a viable strategy to extrapolate quantitative information on the impact of the Cys-N degron pathway on hypoxic gene expression that would be difficult to extract from the native plant host, using genetic approaches. Moreover, the minimal MynOx circuit constitutes a unique orthogonal switch controlled by hypoxia that may be further exploited to introduce oxygen-dependent responses in yeast.

Materials and Methods

Plant Material. Col-0 *A. thaliana* was used as wild-type. The pentuple *erfVII* mutant (33) and the overexpressing line *35S:RAP2.3*^{3xHA} (35) were kindly provided by Mike Holdsworth. The $HRPE_{ADH}$*:NLUC* reporter line was described by (42). Seven day-old Arabidopsis seedlings were subjected to hypoxic or chemical treatments. Plants were grown on 2.15 g L^{-1} MS medium (Duchefa) supplemented with 10 g L^{-1} sucrose, either in 6-well plates, or vertical plates in presence of 9 g L^{-1} agar, as described previously in (80). Transient expression of SYRAP and UbSYRAP constructs was accomplished by agroinfiltration of three week-old $HRPE_{ADH}$*:NLUC* plants, according to (39). Three days after infiltration, leaves were excised and incubated in 1 mL of water under normoxic or hypoxic conditions, with 150 rpm shaking and 23 °C in the dark.

Yeast Strains, Culture, and Transformation. The haploid *S. cerevisiae* strains MaV203 (Thermo-Fisher Scientific #11445012), W303 1A (*MATa*) and W303 1B (*MATα*) (Scientific Research and Development, GmbH, #20000A and #20000B) were used. Fresh cells from YPDA plates were transformed following the PEG/LiAc/SS DNA method (81). A detailed transformation protocol is described in *SI Appendix, Extended Methods*. All strains generated in this study are listed in *SI Appendix*, Table S6. Unless differently specified, yeast was grown on synthetic yeast dropout (SD) medium, with appropriate supplements, as described in (27). Spots were prepared from exponential cultures (OD_{600} = 0.75). Approximately 10^5 cells were spotted on solid SD medium (-his-trp-leu-ura) and grown for 28 h at 30 °C prior to treatments. For gene expression and luciferase measurements, cells were sampled by gently scratching the surface of colonies, avoiding contaminations with the agar, resuspended in a tube and flash frozen.

Cloning of Yeast and Plant Components. Entry vectors were generated by Gateway BP Clonase reaction between pDONR201 (Thermo Fisher Scientific) and attB containing inserts. Strings were synthesized through GeneArt® (Thermo-Fisher Scientific), *SI Appendix*, Table S7. Cloning procedures and sequence information of the inserts can be found in *SI Appendix, Extended Methods*, and the specific primers used in *SI Appendix*, Table S8. Entry plasmids (*SI Appendix*, Table S9) were recombined into suitable destination vectors using the Gateway™ LR Clonase™ II Enzyme mix (Thermo-Fisher Scientific). Combinations of yeast expression vectors were transformed into the different yeast strains as detailed in *SI Appendix*, Table S7.

Low Oxygen Treatments. Treatments were carried out in a sealed hypoxic glovebox with temperature control (Coy Lab Products). Arabidopsis seedlings and leaves were kept in the dark at 23 °C, under 120 rpm continuous shaking, for the duration of the hypoxic treatment. The plant material was sampled inside the glovebox by flash freezing in liquid nitrogen.

Hypoxia was applied to diluted yeast suspensions dispensed in 200 µL volume in 96-well plates (microcultures), or to 5- or 10-mL cultures in individual vials, as specified for the different experiments. The treatments consisted in the incubation under 1% O_2 atmosphere (v/v), at 30 °C and with 150 rpm shaking. Culture production and handling has been described before (80). In "hypoxic chase" experiments, media were pre-equilibrated with the hypoxic atmosphere in the glovebox, set at the desired O_2 concentration (10% or 1% O_2 v/v). Five mL cultures diluted to OD_{600} = 0.1 were first pregrown for 5 h in aerated conditions to exponential phase, then recovered by centrifugation (5,000×*g*, 2 min) and resuspended in the same volume of pre-equilibrated media directly inside the hypoxic glovebox. For the duration of the treatment, O_2 concentration in the media was measured with a FireSting®-GO2 m (PyroScience), thanks to a fluorescent oxygen sensor spot (OXSP5, PyroScience) attached inside the container with the medium. Dissolved O_2 was also monitored in the same way inside a separate culture for the duration of the treatment, to ensure the maintenance of steady-state O_2 levels across all sampling points (43).

Reporter Assays. Luciferase activity was assessed with the aid of commercial kits, following the manufacturer's recommendations. Approximately 5 × 10^5 yeast cells were harvested from growing cultures or spots, flash frozen in N_2 and resuspended in 150 µL Passive Lysis Buffer (PLB, Promega). NLUC activity was measured and normalized to FLUC activity (NLUC/FLUC) using the Nano-Glo® Dual Luciferase Assay System (Promega). In the case of Arabidopsis samples, 15 seedlings or one agroinfiltrated leaf were frozen, ground to fine powder with mortar and pestle and suspended in 1 mL PLB. NLUC signal was measured with the Nano-Glo® Luciferase Assay System (Promega) and normalized to the amount of total proteins, quantified using the Pierce™ BCA Protein Assay Kit (Thermo-Fisher Scientific). DLOR activity was measured as described in (27) using the Dual-Luciferase® Reporter Assay System (Promega). Detailed information on the UAS_{GAL} activation experiments performed in MaV203 strains is provided in *SI Appendix, Extended Methods*.

Gene Expression Analyses. Total RNA was isolated from Arabidopsis samples as described before (18) and from yeast samples as described in (80). One µg total RNA was processed to cDNA with the Maxima cDNA synthesis kit (Thermo-Fisher Scientific), according to the manufacturer's protocol. Real-time qPCR was performed with 12.5 ng cDNA template, using the PowerUp SYBR® Green Master Mix (Thermo-Fisher Scientific) and a CFX384 detection system (Bio-Rad). Gene-specific qPCR primers are listed in *SI Appendix*, Table S10. Gene expression was expressed as relative to the yeast housekeeping gene *ACT1* (YFL039C) and the Arabidopsis housekeeping *UBQ10* (At4g05320), through the comparative ΔΔCt method (82).

Immunoblotting. Detailed information on protein extraction from plant and yeast material, immunoblotting, and detection is provided in *SI Appendix, Extended Methods*.

Promoter Analysis. The intergenic regions upstream of ATG of the nine selected HRGs (*ADH1, HRA1, PDC1, PGB1, PCO1, LBD41, HRE2, SAD6,* and *SUS4*) were extracted using Integrated Genome Browser® (v. 10.0). The individual motif occurrence tool FIMO (https://meme-suite.org/meme/tools/fimo) was used to find Hypoxia Response Promoter Elements (HRPEs) from the available consensus sequences (30) with a filtering *P*-value of 0.001 for positive hits.

Mathematical Modeling of NLUC, UbSYRAP, and PCO1/4 Kinetics. Detailed information on the modeling process is provided in *SI Appendix, Extended Methods*. The models used were deposited on GitHub (83).

Data Representation and Statistics. Detailed information is provided in *SI Appendix, Extended Methods*.

Data, Materials, and Software Availability. Plasmids were deposited at Addgene (84), and the code is available on GitHub (85). All other data are included in the article and/or *SI Appendix*.

ACKNOWLEDGMENTS. We would like to thank Prof. Pierdomenico Perata for his suggestions and support during the early development of this project and Beatriz Pasero Garcia for her help and insight on the promoter analysis. This work was partially supported by the UKRI Biotechnology and Biological Science Research Council Pioneer Award Grant BB/Y512953/1, to M.L.-P. and F.L., and by the European Research Council (ERC) Grant 101001320, to F.L. Y.H. was supported by the Biotechnology and Biological Sciences Research Council (BBSRC) Grant BB/T008784/1. A.P. was supported by the Engineering and Physical Sciences Research Council (EPSRC) Grants EP/Y014073/1, EP/X031470/1, and UKRI2108.

1. Y. Y. Jiang *et al.*, The impact of oxygen on metabolic evolution: A chemoinformatic investigation. *PLoS Comput. Biol.* **8**, 1–8 (2012).
2. E. U. Hammarlund, E. Flashman, S. Mohlin, F. Licausi, Oxygen-sensing mechanisms across eukaryotic kingdoms and their roles in complex multicellularity. *Science* **370**, eaba3512 (2020).
3. M. Becerra *et al.*, The yeast transcriptome in aerobic and hypoxic conditions: Effects of hap1, rox1, rox3 and srb10 deletions. *Mol. Microbiol.* **43**, 545–555 (2002).
4. T. A. Trendeleva, D. A. Aliverdieva, R. A. Zvyagilskaya, Mechanisms of sensing and adaptive responses to low oxygen conditions in mammals and yeasts. *Biochemistry (Mosc.).* **79**, 750–760 (2014).
5. A. Zubrycka *et al.*, ERFVII action and modulation through oxygen-sensing in *Arabidopsis thaliana*. *Nat. Commun.* **14**, 4665 (2023).
6. L. Dalle Carbonare *et al.*, ERFVIIs as transducers of oxygen-sensing in the evolution of land plant response to hypoxia. *Mol. Plant.* **18**, 1072–1087 (2025).
7. F. Licausi *et al.*, Hypoxia responsive gene expression is mediated by various subsets of transcription factors and miRNAs that are determined by the actual oxygen availability. *New Phytol.* **190**, 442–456 (2010).
8. Y. Yao, X. Chen, A. M. Wu, ERF-VII members exhibit synergistic and separate roles in *Arabidopsis*. *Plant Signal Behav* **12**, e1329073 (2017).
9. F. Licausi *et al.*, Oxygen sensing in plants is mediated by an N-end rule pathway for protein destabilization. *Nature* **479**, 419–422 (2011).
10. D. J. Gibbs *et al.*, Homeostatic response to hypoxia is regulated by the N-end rule pathway in plants. *Nature* **479**, 415–418 (2011).
11. K. T. Nguyen, J. M. Kim, S. E. Park, C. S. Hwang, N-terminal methionine excision of proteins creates tertiary destabilizing N-degrons of the Arg/N-end rule pathway. *J. Biol. Chem.* **294**, 4464–4476 (2019).
12. M. D. White, J. J. A. G. Kamps, S. East, L. J. Taylor Kearney, E. Flashman, The plant cysteine oxidases from *Arabidopsis thaliana* are kinetically tailored to act as oxygen sensors. *J. Biol. Chem.* **293**, 11786–11795 (2018).
13. D. M. Gunawardana, K. C. Heathcote, E. Flashman, Emerging roles for thiol dioxygenases as oxygen sensors. *FEBS J.* **289**, 5426–5439 (2022).
14. H. Zhang *et al.*, BIG enhances Arg/N-degron pathway-mediated protein degradation to regulate Arabidopsis hypoxia responses and suberin deposition. *Plant Cell* **36**, 3177–3200 (2024), 10.1093/plcell/koae117/7644967.
15. N. Masson *et al.*, Conserved N-terminal cysteine dioxygenases transduce responses to hypoxia in animals and plants. *Science* **1979**, 65–69 (2019).
16. P. Barreto *et al.*, Mitochondrial retrograde signaling through UCP1-mediated inhibition of the plant oxygen-sensing pathway. *Curr. Biol.* **32**, 1403–1411.e4 (2022).
17. Y. Zhou *et al.*, Polyunsaturated linolenoyl-CoA modulates ERF-VII–mediated hypoxia signaling in Arabidopsis. *J. Integr. Plant Biol.* **62**, 330–348 (2020).
18. M. Kosmacz *et al.*, The stability and nuclear localization of the transcription factor RAP2.12 are dynamically regulated by oxygen concentration. *Plant Cell Environ.* **38**, 1094–1103 (2015).
19. R. R. Schmidt *et al.*, Low-oxygen response is triggered by an ATP-dependent shift in oleoyl-CoA in *Arabidopsis*. *Proc. Natl. Acad. Sci.* **115**, E12101–E12110 (2018).
20. B. Fan *et al.*, Calcium-dependent activation of CPK12 facilitates its cytoplasm-to-nucleus translocation to potentiate plant hypoxia sensing by phosphorylating ERF-VII transcription factors. *Mol. Plant.* **16**, 979–998 (2023).
21. A. B. Kunkowska *et al.*, Target of rapamycin signaling couples energy to oxygen sensing to modulate hypoxic gene expression in Arabidopsis. *Proc. Natl. Acad. Sci. U.S.A.* **120**, e2212474120 (2023).
22. I. De Clercq *et al.*, The membrane-bound NAC transcription factor ANAC013 functions in mitochondrial retrograde regulation of the oxidative stress response in Arabidopsis. *Plant Cell* **25**, 3472–3490 (2013).
23. E. Eyshold-Derzsò *et al.*, Endoplasmic reticulum–bound ANAC013 factor is cleaved by RHOMBOID-LIKE 2 during the initial response to hypoxia in. *Proc. Natl. Acad. Sci. U.S.A.* **120**, 2017 (2023).
24. A. Mustroph *et al.*, Profiling translatomes of discrete cell populations resolves altered cellular priorities during hypoxia in Arabidopsis. *Proc. Natl. Acad. Sci. U.S.A.* **106**, 18843–18848 (2009).
25. E. Eysholdt-Derzsó *et al.*, Endoplasmic reticulum–bound ANAC013 factor is cleaved by RHOMBOID-LIKE 2 during the initial response to hypoxia in *Arabidopsis thaliana*. *Proc. Natl. Acad. Sci. U.S.A.* **120**, e2221308120 (2023).
26. E. Andrianantoandro, S. Basu, D. K. Karig, R. Weiss, Synthetic biology: New engineering rules for an emerging discipline. *Mol. Syst. Biol.* **2**, 0028 (2006).
27. M. L. Puerta *et al.*, A ratiometric sensor based on plant N-terminal degrons able to report oxygen dynamics in *Saccharomyces cerevisiae*. *J. Mol. Biol.* **431**, 2810–2820 (2019).
28. A. Mustroph *et al.*, Cross-kingdom comparison of transcriptomic adjustments to low-oxygen stress highlights conserved and plant-specific responses. *Plant Physiol.* **152**, 1484–1500 (2010).
29. F. Liu *et al.*, Global transcription profiling reveals comprehensive insights into hypoxic response in *Arabidopsis*. *Plant Physiol.* **137**, 1115–1129 (2005).
30. P. Gasch *et al.*, Redundant ERF-VII transcription factors bind to an evolutionarily conserved cis-motif to regulate hypoxia-responsive gene expression in *Arabidopsis*. *Plant Cell* **28**, 160–180 (2016).
31. R. Azen, D. V. Budescu, The dominance analysis approach for comparing predictors in multiple regression. *Psychol. Methods* **8**, 129–148 (2003).
32. D. V. Budescu, Dominance analysis: A new approach to the problem of relative importance of predictors in multiple regression. *Psychol. Bull.* 114, 542–551 (1993).
33. M. Abbas *et al.*, Oxygen sensing coordinates photomorphogenesis to facilitate seedling survival. *Curr. Biol.* **25**, 1483–1488 (2015).
34. B. Giuntoli *et al.*, Age-dependent regulation of ERF-VII transcription factor activity in *Arabidopsis thaliana*. *Plant Cell Environ.* **40**, 2333–2346 (2017).
35. D. J. Gibbs *et al.*, Nitric oxide sensing in plants is mediated by proteolytic control of group VII erf transcription factors. *Mol. Cell* **53**, 369–379 (2014).
36. T. A. Lee, J. Bailey-Serres, Integrative analysis from the epigenome to translatome uncovers patterns of dominant nuclear regulation during transient stress. *Plant Cell* **31**, 2573–2595 (2019).
37. N. Gaspar *et al.*, Evaluation of NanoLuc substrates for bioluminescence imaging of transferred cells in mice. *J. Photochem. Photobiol. B.* **216**, 112128 (2021).
38. D. A. Weits *et al.*, An apical hypoxic niche sets the pace of shoot meristem activity. *Nature* **569**, 714–717 (2019).
39. G. Panicucci, S. Iacopino, E. De Meo, P. Perata, D. A. Weits, An improved HRPE-based transcriptional output reporter to detect hypoxia and anoxia in plant tissue. *Biosensors* **10**, 197 (2020).
40. P. R. Kumar, Y. Yu, R. Sternglanz, S. A. Johnston, L. Joshua-Tor, NADP regulates the yeast GAL induction system. *Science* **1979**, 1090–1092 (2008).
41. D. Cortens *et al.*, A deeper understanding of the spontaneous derepression of the *URA3* gene in MaV203 *Saccharomyces cerevisiae* and its implications for protein engineering and the reverse two-hybrid system. *Yeast* **36**, 701–710 (2019).
42. S. Akter *et al.*, H_2O_2 repurposes the plant oxygen-sensing machinery to control the transcriptional response to oxidative stress. bioXriv [Preprint] (2024), 10.1101/2024.10.21.619351 (Accessed 1 December 2025).
43. M. Lavilla-Puerta, B. Giuntoli, "Assessing in vivo oxygen dynamics using plant N-terminal degrons in *Saccharomyces cerevisiae*" in *Methods in Molecular Biology* (2022), pp. 269–286.
44. C. Branco-Price, K. A. Kaiser, C. J. H. Jang, C. K. Larive, J. Bailey-Serres, Selective mRNA translation coordinates energetic and metabolic adjustments to cellular oxygen deprivation and reoxygenation in *Arabidopsis thaliana*. *Plant J.* **56**, 743–755 (2008).
45. L. Liu, Y. Zhang, Z. Liu, D. Petranovic, J. Nielsen, Improving heterologous protein secretion at aerobic conditions by activating hypoxia-induced genes in *Saccharomyces cerevisiae*. *FEMS Yeast Res.* **15**, fov070 (2015).
46. A. Riba *et al.*, Protein synthesis rates and ribosome occupancies reveal determinants of translation elongation rates. *Proc. Natl. Acad. Sci. U.S.A.* **116**, 15023–15032 (2019).
47. D. A. Weits *et al.*, Acquisition of hypoxia inducibility by oxygen sensing N-terminal cysteine oxidase in spermatophytes. *Plant Cell Environ.* **46**, 322–338 (2023).
48. F. Licausi *et al.*, HRE1 and HRE2, two hypoxia-inducible ethylene response factors, affect anaerobic responses in *Arabidopsis thaliana*. *Plant J.* **62**, 302–315 (2010).
49. F. Wang, Z. H. Chen, S. Shabala, Hypoxia sensing in plants: On a quest for ion channels as putative oxygen sensors. *Plant Cell Physiol.* **58**, 1126–1142, Preprint (2017).
50. J. T. Van Dongen *et al.*, Transcript and metabolite profiling of the adaptive response to mild decreases in oxygen concentration in the roots of Arabidopsis plants. *Ann. Bot.* **103**, 269–280 (2009).
51. B. Giuntoli *et al.*, A trihelix DNA binding protein counterbalances hypoxia-responsive transcriptional activation in Arabidopsis. *PLoS Biol.* **12**, e1001950 (2014).
52. D. J. Gibbs, F. L. Theodoulou, J. Bailey-Serres, Primed to persevere: Hypoxia regulation from epigenome to protein accumulation in plants. *Plant Physiol.* **197**, kiae584 (2025).
53. S. Castellana, P. M. Triozzi, M. Dell'Acqua, E. Loreti, P. Perata, Environmental genome-wide association studies across precipitation regimes reveal that the E3 ubiquitin ligase MBR1 regulates plant adaptation to rainy environments. *Plant Commun.* **5**, 101074 (2024).

54. V. Shukla *et al.*, Endogenous hypoxia in lateral root primordia controls root architecture by antagonizing auxin signaling in Arabidopsis. *Mol. Plant.* **12**, 538–551 (2019).
55. J. Vicente *et al.*, The Cys-Arg/N-end rule pathway is a general sensor of abiotic stress in flowering plants. *Curr. Biol.* **27**, 3183–3190.e4 (2017).
56. I. Whitehouse *et al.*, Nucleosome mobilization catalysed by the yeast SWI/SNF complex. *Nature* **400**, 784–787 (1999).
57. H. Zhang, D. N. Roberts, B. R. Cairns, Genome-wide dynamics of Htz1, a histone H2A variant that poises repressed/basal promoters for activation through histone loss. *Cell* **123**, 219–231 (2005).
58. M. Lavilla-Puerta, B. Giuntoli, Designed to breathe: Synthetic biology applications in plant hypoxia. *Plant Physiol.* **197**, kiae623 (2025).
59. M. Avdovic, M. Garcia-Navarret, D. Ruiz-Sanchi, K. Wabnik, Dynamic context-dependent regulation of auxin feedback signaling in synthetic gene circuits. *Proc. Natl. Acad. Sci. U.S.A.* **120**, e2309007120 (2023).
60. G. Naseri *et al.*, Plant-derived transcription factors for orthologous regulation of gene expression in the yeast *Saccharomyces cerevisiae*. *ACS Synth. Biol.* **6**, 1742–1756 (2017).
61. E. Pierre-Jerome, S. S. Jang, K. A. Havens, J. L. Nemhauser, E. Klavins, Recapitulation of the forward nuclear auxin response pathway in yeast. *Proc. Natl. Acad. Sci. U.S.A.* **111**, 9407–9412 (2014).
62. P. D'hooge *et al.*, Ca2+ homeostasis in the budding yeast Saccharomyces cerevisiae: Impact of ER/Golgi Ca2+ storage. *Cell Calcium* **58**, 226–235 (2015).
63. J. H. M. Schippers *et al.*, ERFVII-controlled hypoxia responses are in part facilitated by mediator subunit 25 in *Arabidopsis thaliana*. *Plant J.* **120**, 748–768 (2024).
64. D. S. M. Ottoz, F. Rudolf, J. Stelling, Inducible, tightly regulated and growth condition-independent transcription factor in Saccharomyces cerevisiae. *Nucleic Acids Res.* **42**, e130–e130 (2014).
65. S. C. Amack, M. S. Antunes, CaMV35S promoter – A plant biology and biotechnology workhorse in the era of synthetic biology. *Curr. Plant Biol.* **24**, 100179 (2020).
66. A. D. Basehoar, S. J. Zanton, B. F. Pugh, Identification and Distinct Regulation of Yeast TATA Box-Containing Genes. *Cell*. 116, 699–709 (2004).
67. J. Riith, H. Hirt, R. Schweyen, The cauliflower mosaic virus 35S promoter is regulated by cAMP in *Saccharomyces cerevisiae*. *Mol. Gen. Genet.* 235, 365–372 (1992).
68. F. De Amicis, T. Patti, S. Marchetti, Improvement of the pBI121 plant expression vector by leader replacement with a sequence combining a poly(CAA) and a CT motif. *Transgenic Res.* **16**, 731–738 (2007).
69. S. Dvir *et al.*, Deciphering the rules by which 5′-UTR sequences affect protein expression in yeast. *Proc. Natl. Acad. Sci. U.S.A.* **110**, E2792–E2801 (2013).
70. J. T. Cuperus *et al.*, Deep learning of the regulatory grammar of yeast 5′ untranslated regions from 500, 000 random sequences. *Genome Res.* **27**, 2015–2024 (2017).
71. D. A. Weits *et al.*, Plant cysteine oxidases control the oxygen-dependent branch of the N-end-rule pathway. *Nat. Commun.* **5**, 1–10 (2014).
72. R. C. Brewster *et al.*, The transcription factor titration effect dictates level of gene expression. *Cell* **156**, 1312–1323 (2014).
73. L. Wei *et al.*, Regulation by competition: A hidden layer of gene regulatory network. *Quant. Biol.* **7**, 110–121 (2019).
74. A. Y. Weiße, D. A. Oyarzún, V. Danos, P. S. Swain, Mechanistic links between cellular trade-offs, gene expression, and growth. *Proc. Natl. Acad. Sci. U.S.A.* **112**, E1038–E1047 (2015).
75. S. Grossberg, Biological competition: Decision rules, pattern formation, and oscillations. *Proc. Natl. Acad. Sci. U.S.A.* **77**, 2338–2342 (1980).
76. A. J. Genot, T. Fujii, Y. Rondelez, Scaling down DNA circuits with competitive neural networks. *J. R. Soc. Interface* **10**, 20130212 (2013).
77. A. Burger, A. M. Walczak, P. G. Wolynes, Abduction and asylum in the lives of transcription factors. *Proc. Natl. Acad. Sci. U.S.A.* **107**, 4016–4021 (2010).
78. I. J. Higgins, S. G. Choudury, A. Y. Husbands, Mechanisms driving functional divergence of transcription factor paralogs. *New Phytol.* **247**, 2022–2033 (2025).
79. Y. Zhang, T. D. Ho, N. E. Buchler, R. Gordân, Competition for DNA binding between paralogous transcription factors determines their genomic occupancy and regulatory functions. *Genome Res.* **31**, 1216–1229 (2021).
80. M. Lavilla-Puerta *et al.*, Identification of novel plant cysteine oxidase inhibitors from a yeast chemical genetic screen. *J. Biol. Chem.* **299**, 105366 (2023).
81. R. D. Gietz, R. H. Schiestl, High-efficiency yeast transformation using the LiAc/SS carrier DNA/PEG method. *Nat. Protoc.* **2**, 31–34 (2007).
82. H. Kai, F. Huiyun, Analysis of relative gene expression data using real- time quantitative PCR and the 2-DDCT method. *Methods* **25**, 402–408 (2001).
83. M. Lavilla-Puerta *et al.*, A synthetic ERFVII-dependent circuit in yeast sheds light on the regulation of early hypoxic responses of plants. https://doi.org/10.5281/zenodo.18771150. Deposited 25 February 2026.
84. M. Lavilla-Puerta *et al.*, A synthetic ERFVII-dependent circuit in yeast sheds light on the regulation of early hypoxic responses of plants. Addgene. https://www.addgene.org/browse/article/28263658/. Deposited 9 February 2026.
85. Y. He, MATLAB and R code for reproducibility. GitHub. https://github.com/ymiplant/synthetic-erfvii-yeast-hypoxia/tree/main. Deposited 25 February 2026.